Enhancement of Pool Boiling Heat Transfer using Nanostructured Surfaces on Aluminum and Copper

Terry J. Hendricks[⊥], Shankar Krishnan
Battelle/Pacific Northwest National Laboratory
MicroProducts Breakthrough Institute
1000 NE Circle Boulevard, Suite 11101
Corvallis, OR – 97330

Changho Choi, Chih-hung Chang
School of Chemical, Biological, and Environmental Engineering
Oregon State University
Corvallis, OR – 97331

Brian Paul
School of Mechanical, Industrial, and Manufacturing Engineering
Oregon State University
Corvallis, OR - 97331

ABSTRACT

Enhanced pool boiling critical heat fluxes (CHF) at reduced wall superheat on nanostructured substrates are reported. Nanostructured surfaces were realized using a low temperature process, microreactor-assisted-nanomaterial-deposition. Using this technique we deposited ZnO nano-structures on Al and Cu substrates. We observed pool boiling CHF of 82.5 W/cm^2 with water as fluid for ZnO on Al versus a CHF of 23.2 W/cm^2 on bare Al surface with a wall superheat reduction of 25-38 °C. These CHF values on ZnO surfaces correspond to a heat transfer coefficient of ~ 23000 W/m^{2}K. We discuss our data and compare the behavior with conventional boiling theory.

Keywords: nanoscale heat transfer, boiling enhancement, electronic cooling

[⊥] Corresponding author (terry.hendricks@pnl.gov)

NOMENCLATURE

English

A – Heater Area [m^2]
C_p - Liquid Specific Heat [J/kg-K]
D_b – Vapor Bubble Diameter [m]
f - Bubble Departure Frequency [1/second or Hertz]
g – gravitational acceleration, [m/s^2]
h_{fg} – Enthalpy of Vaporization [J/kg]
I – Current [I]
K - Empirical Constant in Eq. [1]
k_l - Liquid Thermal Conductivity [W/m-K]
N_a - Bubble Nucleation Site Density [$1/m^2$ or $1/cm^2$]
q'' – Surface Heat Flux [W/m^2 or W/cm^2]
R_c – Cavity Radius, [m]
t – Time [seconds]
T_s - Boiling Surface Temperature [K]
T_{sat} - Boiling Liquid Saturation Temperature [K]
V – Voltage [V]

Greek

ρ - Liquid Density [kg/m^3]
ρ_g - Vapor or Gas Density [kg/m^3]
ΔT_w – Surface or Wall Superheat ($T_{surf} - T_{sat}$) [K]
π - Standard Mathematical pi, 3.14159…
θ - Contact Angle [Degrees]
σ - Surface Tension [N/m]

Subscripts

b - Bubble
c – Cavity
d – Bubble departure point in time
f - Liquid
g – Vapor or gas
l – Liquid conditions
sat – Saturation temperature conditions
w – Bubble initiation waiting period

INTRODUCTION

Electronic system energy management and cooling for future advanced lasers, radars, and power electronics is gaining importance, resulting in requirements for technologies and design techniques to dissipate ultra-high heat fluxes, reduce system energy usage, and increase system efficiencies. There is a general requirement to develop compact, light-weight, and low-cost thermal control and heat exchange systems. Therefore, in almost all applications the heat

exchange systems must satisfy general requirements to transfer very high heat fluxes (i.e., 200-1000 W/cm^2) across nearly isothermal material conditions in high performance computers, advanced military avionics, power devices, electric vehicles and energy recovery systems [1,2]. Various advanced laser, advanced radar, and power electronics technologies will require high performance heat transfer characteristics typical of micro-channel heat exchangers to achieve performance targets and requirements. Advanced power electronics are working toward packages that require thermal control systems capable of providing cooling heat fluxes of about 200 W/cm^2 to maintain die-level (i.e., capacitors, diodes, transistors, CMOS) temperatures within a critical maximum. Advanced radar systems use large amounts of power and tend to operate at higher temperatures than desired under high power output conditions. Cooling heat fluxes in these applications are generally greater than 1000 W/cm^2. Mudawar [1] discusses directed energy devices like high-efficiency, multi-megawatt, continuous wave magnetrons in short-pulse lasers and radar systems that have cooling heat flux requirements of near 10,000 W/cm^2.

In order to accommodate heat flux levels of 1000-10,000 W/cm^2, such as those discussed by Qu and Mudawar [1,3], two phase-flow cooling systems will be required and must be designed in various configurations. Processing gases and liquids together in microchannels having at least one dimension <1 mm has unique advantages for rapid heat and mass transfer. A microchannel heat sink possesses many unique attributes that are ideally suited for cooling ultra-high heat fluxes. Those include compactness, superior heat transfer characteristics because of thin fluid boundary layers with fast fluid acceleration, and minimal coolant usage, especially when the coolant changes phase inside the channels. Phase change capitalizes upon the coolant's latent heat of vaporization to absorb and dissipate a larger amount of heat than a single-phase coolant. Moreover, the heat is removed at a fairly constant temperature that is dictated fundamentally by the coolant's saturation temperature.

Two-phase flow behavior and effects (i.e. heat transfer and pressure drop) in microchannel configurations are not completely understood and have been investigated by a number of researchers [4,5,6,7,8]. Celata et al. [4] have shown that critical heat fluxes as high as 1500-10,000 W/cm^2 are possible with flow boiling of water in microchannel configurations. The ultra-high heat fluxes possible [4] provide critical motivation for this work, including those cooling applications associated with the most-stringent short-pulsed laser and radar requirements discussed above.

Nano-textured surface effects on two-phase heat transfer and boiling are even more in their infancy. Recently, there has been an increased interest in evaluating the pool-boiling performance of nanowire/nanotube surfaces [9,10,11,12]. They have found enhanced pool boiling heat fluxes (2-3X) on nano-coated surfaces against bare substrates. This work aims to demonstrate and quantify enhancement of boiling by unique micro-/nano-structuring on bare surfaces, created using MAND processes, to cool ultra-high heat fluxes for lasers, radars, and power electronics. Surface wettability characteristics are modulated to enable capillary-pressure-assisted liquid flow path to evaporation zones with minimal resistance to vapor escape. These nanostructured surfaces are capable of providing an increase in critical heat fluxes (CHF) and a reduction in surface superheat. This paper discusses our novel approach to fabricate unique nanostructured surfaces using ZnO and discuss pool boiling heat transfer on these surfaces.

NANOSTRUCTURED SURFACES: MAND^{TM}

The boiling process generally depends on and is enhanced by three factors: 1) Existence of random micro or nano-size crevices and surface irregularities for nucleation initiation, 2) a somewhat porous surface structure that allows fluid inflow to keep nucleation sites active, and 3) surface protrusions that create more active boiling area. The nucleate pool-boiling process is described using several bubble dynamics characteristics, such as the vapor bubble diameter at the moment of departure, D_b, the vapor bubble departure frequency, f, mean velocity of vapor bubble growth, D_bf, and the surface characteristics [13]. However, in practice, these characteristics are very difficult to measure owing to the stochastic nature of the boiling process. It is known from conventional theory [13] that the average heat flux dissipated due to nucleate boiling can be related as:

$$q'' = K(\pi(k_l\sigma C_p)\, f)^{0.5} D_b^2 N_a \Delta T_w \qquad (1)$$

where k_l,C_p and σ are the liquid thermal conductivity, specific heat and surface tension, respectively. K is a constant that represents the bubble diameter of influence and is independent of contact angle and physical properties of the fluid. Here, D_b and f are defined above and N_a is nucleation site density. For "bare" surfaces, the nucleation site density is estimated by the relation [13]:

$$\sqrt{N_a} = 25 \times 10^{-8} \left(\frac{h_{fg} \rho_g \Delta T}{T_s \sigma} \right) \quad (2)$$

It is believed that for nanostructured surfaces the product of $f^{0.5}D_b^2N_a$ will increase significantly due to increased site density and concomitant increase in bubble frequency and provide boiling enhancement. The critical heat flux limit of any evaporating system depends on the mechanisms of liquid supply to and vapor escape from the phase change interface and therefore can be rationalized to be limited by the liquid and vapor flow resistances [14]. A theoretical CHF maximum was derived by Gambill and Lienhard [14] based on the vapor resistance dictated by the kinetic limits. For water at atmospheric conditions, the kinetic limit of evaporation is $O(10^4)$ W/cm^2, which is larger by two orders of magnitude than that typically observed in practice for pool boiling. But, this shows that there is much room for enhancement by co-designing effective liquid supply and evaporative zones.

This work has developed a novel solution-based deposition process, MAND^{TM}, which makes use of a microreactor to control the deposition reacting flux. Microreactor-assisted nanomaterial deposition (MAND^{TM}) techniques [15,16] are capable of producing nano-textured features exhibiting the three important characteristics discussed above (see Figures 1 and 2). This work demonstrated the capability to control MAND^{TM} processes to create both hydrophillic (contact angle~50-60°) ZnO surfaces and superhydrophillic ZnO surfaces (contact angle<20°) shown in Figure 2 by simple changes to MAND^{TM} process parameters (i.e., NaOH concentrations and residence time). Simultaneously, our microreactors also have demonstrated dramatic enhancements in controlling nanoparticle size distributions and nanostructured shape effects [17,18,19]. These results suggest the possibility of many types of selectively engineered, nanostructured patterns to enhance boiling behavior using low cost solution chemistries and processes. As solution processes, MAND^{TM} approaches are less expensive than carbon nanotube approaches and more importantly processing temperatures are low.

MAND^{TM} processes provide the potential to greatly reduce the costs, environmental impacts and safety risks associated with the manufacturing of nano-enabled products. In deposition, microreactors provide temporal control over reaction chemistries enabling access to short-life reagents capable of reducing cycle times and costs while improving energy and material efficiencies. Further, Oregon State University researchers has demonstrated the heterogeneous nucleation and growth of nanostructured surfaces from short-life reaction chemistries leading to

shorter cycle times with improved energy and material efficiencies [20,21]. Overall, OSU has demonstrated significant economical and environmental advantages of MAND^{TM} processes over existing vapor-phase deposition techniques [22,23]. From a detailed literature search, MAND^{TM} type approaches have not been systematically explored to date for thermal applications.

Aluminum, silicon and copper substrates are most commonly used in advanced electronics cooling and therefore highly transferable to those types of applications. A variety of different ZnO nanostructures were deposited on these substrates using a rotating-disk MAND process. The deposition was performed at 2000 rpm using a solution at 70°C and a substrate temperature at 200°C. Figure 2 shows examples of the nano-deposited structures on aluminum (Figure 2a) and copper substrates (Figure 2b), respectively. Different types of flower-like nanostructures can be clearly observed for the SEM images. Atomic Force Microscopy (AFM) was used to evaluate the surface structures and topology. The ZnO-on-Cu films appear hydrophilic with an average roughness 162.29 nm. Pore sizes for the ZnO-on-Al are 50-100 nm, pore densities are 30-100 /μm^2, and the structures are about 40 nm tall. In the case of ZnO on aluminum and copper, the contact angle was controlled from about 94° to 0° by simple variations in the MAND^{TM} process parameters (i.e., NaOH concentration and residence time).

Our surfaces displayed hydrophillic characteristics and can be explained using the well know Wenzel theory. For a rough surface such as the ones shown in Figure 2, there are typically two equilibrium states in which a wetting drop resides: the drop either wets the grooves (Wenzel state) or sits on the peaks of the rough surfaces (Cassie state). The hydrophillicity of our surfaces can be explained with the Wenzel equation ($\cos \gamma = r \cos \theta$) where r is the roughness factor (ratio of total surface area to total projected surface area), and γ and θ are contact angles on the nanostructured (roughened) and completely smooth surfaces, respectively. Typically, water contact angle on a flat Cu surface is less than 90° (and decreases with higher temperature) due to native oxides formed on the surface, so for the roughened surfaces with nano features ($r>1$ always because of higher surface area) these surfaces become more hydrophilic as can be easily seen by Wenzel equation.

It is known that the work required for vapor bubble creation on non-wetted surfaces ($\theta \sim 180°$) is very small, and the probability of vapor bubble generation tends to be 1. Wang and Dhir [24] experimentally investigated water boiling (at atmospheric pressure) on vertical copper surfaces with different wettabilities and found that the number of active vapor generating centers

decreased as the wettability of the boiling surface improved (i.e., with decreasing contact angles). It is further known that [13]

$$D_b \sim \theta \sqrt{\frac{\sigma}{g(\rho - \rho_g)}} \tag{3}$$

which proposes that bubble diameter decreases with decreasing contact angle θ. This would suggest that the entire boiling curve, and ultimately the CHF, would decrease with contact angle. Further, Liaw and Dhir [25] reported an investigation on contact angle dependence on critical heat flux, in which they found that CHF increased with decreasing contact angles. These two theories represent an opposing CHF dependence on contact angle which creates an unresolved controversy (Dhir, [26] and Theofanous et al., [27]). This aspect of contact angle dependence with respect to nanostructured surfaces will be discussed later in the paper. Micro-reactor techniques are sufficiently adaptable that several material combinations and process refinements are possible in a short time. These tailored surfaces provide high-density nucleation sites, high capillary pumping to boiling sites, easy bubble departure, and high heat transfer surface areas per volume. Figure 2 SEM images are showing the proper characteristics to enhance boiling heat transfer: 1) controllable hydrophobic & hydrophilic characteristics (porous micro- and nano-structures to allow fluid inflow to nucleation sites), 2) high pore densities for enhanced nucleation, and 3) protrusions to increase the active boiling area.

EXPERIMENTAL METHOD

Figure 3 shows the pool boiling facility with a schematic illustration of the heater block instrumentation. The test facility used to evaluate the pool-boiling performance consists of electrical resistive heaters, copper heater block and liquid chamber. The pool boiling chamber is made out of polycarbonate material. Four 50 Ω resistors were soldered to a copper heat spreader of size 9.1 cm^2. Each side of the heater dimensions were approximately 12 times the capillary length of water to avoid modulating hydrodynamic instabilities. Nanostructured boiling surfaces were bonded to the top part of the copper block instrumented with K-type thermocouples as shown in the figure. Two differential temperature thermocouples were also implemented to estimate temperature gradients in the copper block. The entire heating block was then affixed to polycarbonate chamber using a high-temperature RTV. The testing facility (including the

chamber, heating block assembly except for a visual window seen as orange border in Figure 3) was insulated with high-temperature fiber-glass insulation. All the sides of the heating block assembly were insulated to assure one-dimensional heat flow to the boiling surface. Visual images of the boiling process were recorded using a CCD camera. All the electrical input and temperature data were duly recorded using a NI-DAQ system integrated with LABVIEW software in a dedicated computer controlling the boiling heat-transfer experiments.

The heat flux through boiling surface was estimated by measuring the voltage and current across the four 50 Ω resistors externally using two dedicated multimeters (Radioshack) connected to data acquisition system via LABVIEW. The heat flux dissipated is given by the relation:

$$q'' = VI/A \tag{4}$$

where A is the boiling area of the test piece nominally measured to be 9.1 cm^2. Surface temperatures on the boiling surfaces were measured by two K-type thermocouples (Omega Engineering) attached to the top surface using Arctic Silver thermally conductive adhesive (~ 5 W/mK). Water temperature was measured using again two K-type thermocouples as shown in Figure 3.

Heat loss from the boiling set-up was estimated by filling the boiling chamber with fiber glass insulation instead of water thereby forcing the heat to leak through back-side of the heater. Based on the heater temperature versus heater power, it was estimated that heat loss varied from 1.8 W at 50 °C to a maximum of 11.39 W at surface temperatures as high as 220 °C. Using these numbers in actual boiling experiments, the maximum heat loss was about 1.5% of heater power.

Prior to performing the boiling heat-transfer experiments, the samples were characterized to study the structure of the deposited nanostructures. AFM studies were carried out to determine the surface roughness of the deposited ZnO nano-films. The wetting properties of the Al-ZnO and Cu-ZnO were measured. The static contact angles (as a function of residence time) were measured using de-ionized water to evaluate surface wettability at room temperature. A droplet of size 2 μl was placed on the nanostructured surface to measure the contact. The shape of the droplet was captured using a high speed camera, and the contact angle was estimated from the capture image.

Further, a rigorous degassing procedure was adopted prior to carrying out the boiling experiments. De-ionized water was used for all our experiments. Boiled water (using a

microwave oven) was first sonicated for 20 minutes in an ultrasonic bath. Then, the sonicated water was poured into the boiling chamber implemented with two immersion heaters. These immersion heaters were powered on, heater temperatures reached well above 100 °C, and the water was degassed at this power level for about one hour.

After one hour of degassing, the immersion heaters were slowly turned off (10-15 minutes after the start of the actual experiments) while powering on the copper heating block assembly. All experiments were performed at atmospheric pressure and at water saturation temperature. The aim of the experiments was to obtain two key parameters: the wall super heat, $T_s - T_{sat}$, and wall heat flux, q". Experiments were carried out until a critical heat flux (CHF) was reached. At the incipience of CHF, either the wall superheat jumped to very high values or the electrical heaters were burned out.

Repeat tests were performed on selected samples and some of these test results are shown in Figure 4. Table 1 below lists CHF values for repeat tests performed on different nano-structured surfaces. Figure 4 shows typical boiling curves, q", versus surface superheat (i.e., temperature difference between the heated surface and the saturation temperature, T_s - T_{sat}) for two nanostructured surfaces on copper whose contact angles are 30° and 70°, respectively. Detailed boiling curves for a variety of surfaces will be discussed later in this paper. These results in Figure 4 and Table 1 show the repeatability of boiling performance on selected nano-textured surfaces. As can be seen from Figure 4, the copper nano-textured surface (Cu-ZnO-CA-30-FL) whose contact angle was 30° repeated itself with a slightly higher CHF value and lower wall superheat. The other surface (Cu-ZnO-CA-70-FL) displayed lower CHF value and higher wall superheat compared to test 1 upon performing a repeat test. Based on Figure 4 and Table 1, a conclusive picture about the surface degradation after CHF cannot be reached. A detailed study of surface degradation and/or aging was beyond the scope and funding of this work. The authors believe more systematic work is required in this technical area of nanoparticle adhesion to understand the surface degradation characteristics. Nevertheless, efforts are currently underway to ruggedize the nanostructured surfaces.

UNCERTAINTY ANALYSIS

The uncertainty in the heat flux was evaluated using two approaches because the test system had random uncertainties and systematic uncertainties in our test data. The first approach uses

the Kline and McClintock procedure to estimate errors resulting from random uncertainties in voltage and current and the actual size of the boiling area due to substrate cutting. The resulting expression for the relative random uncertainty in heat flux from voltage and current and area is:

$$\frac{\Delta_{q''}}{q''} = \sqrt{\left(\frac{\Delta_V}{V}\right)^2 + \left(\frac{\Delta_I}{I}\right)^2 + \left(\frac{\Delta_A}{A}\right)^2} \tag{5}$$

where Δ represents the uncertainty of the particular quantity indicated by their subscript. The uncertainty for multi-meters to measure voltage and current are 0.8% (4V – 400 V), and 1.2% (less than 4A) or 1.5% (greater than 4 A) with an additional uncertainty of ±4 in last digit, respectively. The estimated uncertainty in the heat flux due to voltage and current is within the range of ±4.0% for all the experimental data reported here.

The systematic uncertainty in our test data is due to measurement of the test sample boiling area and the 1.5% inherent high bias due to heat losses discussed above. The uncertainty in the test sample boiling area is due to two factors: (a) potential coverage of active boiling by a high-temperature epoxy sealant used to affix and seal the boiling surface into the test system, and (b) loss of active boiling area due to thermocouple attachment to the boiling surface. In many experiments, the high temperature epoxy used to affix the heating block assembly in the water chamber overlapped the heater surfaces near the edges by about a 1mm in thickness, which caused a systematic low bias in our heat flux calculations of 8.5%. It also was noticed that boiling generally was absent on Arctic Silver epoxy beads used to hold the thermocouples on top of the heat surfaces, which also caused a systematic high bias in the actual boiling heat transfer area and therefore a systematic low bias in heat flux calculations of about 7.2%.

The random uncertainties and the systematic uncertainties were combined to give an overall total estimated error in the heat fluxes shown in Figures 4 and 5. These overall estimated errors in heat flux were +18% and – 5.5%. The Type K thermocouples used for water and surface temperature measurement have an estimated standard error of 2.2 °C (i.e, ±1.1 °C).

RESULTS AND DISCUSSION

Pool boiling refers to boiling under natural convection and nucleate boiling conditions, where the heating surface is submerged in a large body of stagnant liquid (water is used in our experiments) and the relative motion of the vapor bubble and its surrounding liquid is primarily

due to buoyancy effect. The experimental results were characterized in typical boiling curves plotting the surface heat flux, q", versus surface superheat (i.e., temperature difference between the heated surface and the saturation temperature, $T_s - T_{sat}$). Figure 5 shows the boiling curves, i.e. the dependence of dissipated heat flux on wall superheat , for water, T_{sat} = 100 °C, and compares the performance of various nano-structured surfaces described earlier against bare aluminum in the pool boiling tests . Figure 5 also shows the SEM images of the tested surfaces. Table 2 introduces the legends and average roughness values of nano-textured surfaces shown in Figure 5. Conventional wisdom proposes that nanostructured surfaces will not improve boiling heat transfer because the bubble nucleation process is not expected to be enhanced by very small cavities. But, ZnO nanostructured surfaces displayed all the characteristics of a typical boiling curve where the initial heat transfer process was natural convection limited and ONB (onset of nucleate boiling) was observed as the wall superheat is reached for bubble nucleation. At higher wall superheat, these ZnO nanostructured surfaces activated discrete bubbles on the heater surfaces, PNB (partial nucleate boiling), and transitioned to fully-developed nucleate boiling where the bubbles merge to form vapor columns (see Figure 5). At critical heat flux (CHF), the bubbles are large and merge to form a continuous vapor film between the heater and water. Due to lower thermal conductivity of the vapor compared to liquid water, the thermal resistance increases sharply due to the presence of a vapor film and therefore sets CHF as a practical operation limit. A high CHF value of ~ 82.5 W/cm^2 was observed for the flower-like ZnO nanostructures on Al compared to a bare Al surface CHF of about ~ 23 W/cm^2. This CHF value (82.5 W/cm^2) approaches the maximum CHF value predicted by Hakamura and Katta [31] of 108 W/cm^2. It was further observed these surfaces had lower wall superheat for bubble nucleation compared to a bare Al surface. This work also observed low superheat and a CHF value of 63.5 W/cm^2 for ZnO on Cu with flower morphology (contact angle = 30°). It can be noted from Figure 5 that ZnO nanostructured surfaces display a unique staircase effect in the boiling curves. It was observed that, at certain instances on the curve, the wall superheat would increase steadily while heat flux remaining constant, and then a sudden increase in dissipated heat flux would be observed concomitantly with increasing bubble nucleation population. It is believed that local high superheat activated all the smaller pore-sizes in the neighborhood of a nucleation site. All these high heat flux surfaces exhibited high rates of bubble formation and the nanostructured surfaces were essentially covered in bubbles. This would suggest that very

high bubble frequency and nucleation site density were responsible for the high heat fluxes and high CHF values.

Conventional boiling theory proposes that nanostructured surfaces will not improve boiling heat transfer because the bubble nucleation process is not expected to be enhanced by nano-scale cavities owing to high superheats needed for activation. For example, the minimum cavity mouth radius required for activation, is given by [27]

$$R_c = \frac{2\sigma T_{sat}}{\rho_v h_{fg} \Delta T_s} \tag{6}$$

For a nanosize cavity, ap\]proximately 100 nm and water at saturation, the required superheat is 327 K. But, our experiments have shown enhanced boiling heat transfer on nanostructured surfaces at very low superheats as can be seen in the Figure 5. These data and trends contradict current understanding of bubble nucleation. Previous investigators have also observed similar boiling characteristics on nano-structured surfaces and highly smooth surfaces [9,11,27]. In a recent study by Cavicchi and Avedisian [28] using a transient technique observed presence of meta-stable nanobubbles on hydrophilic surfaces. They observed bubble nucleation upon thermally pulsing surfaces at lower nucleation temperatures owing to the presence of nanobubbles. It might be noted that many researchers have observed nanobubbles on hydrophobic surfaces [29,30]. These studies on presence of nanobubbles on hydrophobic and hydrophilic surfaces indeed support our experimental data on bubble nucleation on nanostructured surfaces.

Qualitatively, it was observed routinely that the ZnO nanostructured surfaces exhibited a high density of bubble formation across the boiling surface throughout the nucleate boiling regime (i.e., after ONB) compared to a simple bare aluminum surface. In addition, nanostructured surfaces with low contact angles (< 10°) seemed to exhibit particularly low bubble formation densities and have difficulty forming bubbles uniformly across the boiling surface. This was routinely manifested in 'high' wall superheats and low CHF values in their boiling curves.

This work observed a CHF dependence on static contact angle as shown in Figure 6. Also, shown in Figure 6 are measured CHF for plain silicon and aluminum surfaces. Current understanding of CHF demarcates two limits: one is surface morphology controlled over a range of contact angles, and the other limit is hydrodynamically controlled (predicted by Zuber relationship [31]) and is relevant to well-wetted surfaces. Furthermore, Chung and No [32] point

out that nucleate boiling models can be used to predict CHF behavior. Some surface morphology controlled theories presented by Wang and Dhir [24], suggesting that the nucleation site density decreases with decreasing contact angle as shown in Eq. (7) below:

$$N_a = 5 \times 10^{-27} (1-\cos\theta)/(2R_c)^6 \quad (7)$$

and Pioro et al. [13], suggesting Eq. (3), would lead one to conclude that the entire boiling curve, and therefore the ultimate CHF, would decrease with decreasing contact angle. The Zuber relationship would predict no contact angle dependence. Other surface morphology related models by Liaw and Dhir [25] and Auracher and Marquardt [33] would suggest that CHF would increase as contact angle decreases. Theofanous et al. [22] discuss the complex interactions during nucleation, bubble dynamics during nucleate boiling, hot spot formation, and ultimately CHF conditions and some of the confusion in this complex technical area. Our measured CHF first increases with decreasing contact angle for the nano-textured flower-like morphology until achieving a maximum CHF for contact angle approximately 18-20°, and then decreased as the contact angle decreased to zero (as clearly seen in Figure 6). A superhydrophillic surface (see Figure 5) of different morphology (carpet like) with contact angle 0° also showed low CHF and also high superheat. Our explanation for this CHF dependence on contact angle with these nano-textured surfaces is that there must be a balance between the surface capillary fluid dynamics that brings fluid into the active nucleation sites and the surface bubble dynamics governed by bubble diameter and nucleation site density that ultimately lead to heat dissipation. The authors surmise that there is an optimum surface wettability condition that optimizes these two competing effects and causes the observed maxima in CHF as contact angle varies. It is known from Carey [31] that bubble frequency can be related to a bubble waiting period, t_w, and bubble growth time to departure, t_d, through the following:

$$(1/f) = t_w + t_d \quad (8)$$

It is hypothesized that the smaller contact angles and therefore better wettability is potentially decreasing the bubble waiting period, t_w, and therefore increasing the bubble nucleation frequency. As the contact angle gets smaller the capillary surface forces increase thereby bringing fluid to active nucleation sites more effectively (thereby potentially increasing bubble frequency), but the bubble diameter decreases (Eq. 3) and number of active nucleation sites decreases as contact angle decreases (per Wang and Dhir [24] and Eq. 7), which therefore ultimately degrades the CHF if contact angle gets too small. These competing effects could lead

to the observed CHF maximum. This hypothesis requires further investigation and experimental verification and new experimental methods to confirm.

As discussed previously, Liaw and Dhir [25] propose that CHF increases with decreasing contact angles, while combining Equations (3) and (1) and the results of Wang and Dhir [24] indicates the opposite effect on boiling heat flux where q" $\rightarrow$ 0 for $\theta \rightarrow 0$. Unfortunately, experimental results for CHF dependence on contact angle for water reported by Liaw and Dhir [25] do not extend to 0° contact angle and are valid only for a range of contact angles from 27° to 107°. However, they did use Zuber's limit to project to a zero contact angle CHF using a relationship that indicates no dependency on contact angle at lower contact angles giving CHF=125 W/cm^2. However, they only experimentally confirmed this with one data point at 0° contact angle using Freon, not water.

The MAND^{TM} process allowed this work the flexibility to investigate contact angles from 0° to near 60° and combine this with results from bare silicon and bare aluminum surfaces. Our results with water included investigating contact angles from 20° to 0° that Liaw and Dhir did not cover. This new information subsequently uncovered that the dependence on contact angle produced the maximum CHF at 20°. In addition, it is noted that one nano-textured surface with a contact angle of 10° was one of the surfaces that was tested twice and repeated its CHF results shown in Figure 4. It is believed that detailed investigation needs to be undertaken to understand the mechanisms causing heat flux augmentation on these nanostructured surfaces, particularly the relationship of surface wettability on bubble frequency, bubble diameter, and nucleation site activation and the effects of surface pore sizes. It might be worth noting that Majumdar and co-workers [9] observed a maxima at a contact angle of 0° (in contrary to a maxima at 20° reported here). This observation might suggest that the upper limit of heat removal might be set by the surface morphology rather than by the hydrodynamics. The work presented here suggests that what is important is the balance between surface fluid dynamics (i.e., including capillarity effects) and surface bubble dynamics, rather than either surface morphology or hydrodynamics alone.

Figure 7 shows heat transfer coefficient (kW/m^{2}K) vs nucleate boiling heat flux (kW/m^2) as a log-log plot of selected surfaces. It is noted that the curves are drawn only for the nucleate

boiling regime. As is clearly seen, compared to a bare Al surface the ZnO nanostructured surfaces show almost an order of magnitude increase in HTC.

The significant increases in both CHF and heat transfer coefficient shown in Figures 5 and 7, respectively, have important and far-reaching ramifications on the use of ZnO nanostructured surfaces for cooling high heat fluxes in advanced power electronics, advanced high-power radar, and advanced laser systems. Work is on-going to investigating the impact of these ZnO nanostructured surfaces on flow boiling environments and configurations, which should exhibit surface heat fluxes in the hundreds of W/cm^2 range. This work has only begun to uncover the potential of the ZnO nanostructured surfaces studied to date. Further experimental and analytical research and development is required to completely understand these phenomena and fully realize the electronic cooling potential of these nanostructured surfaces.

CONCLUSIONS

This work has reported a novel approach to fabricate unique nanostructured surfaces using ZnO on Al and Cu substrates for boiling heat transfer enhancement. It has demonstrated that micro-reactor techniques (MAND^{TM}) are sufficiently adaptable to fabricate tailored surfaces that provides high-density nucleation sites, high capillary pumping to boiling sites, and high heat transfer surface areas per volume.

This work compared rigorous pool-boiling experiments on bare and nanostructured surfaces. Nano-structured surfaces (ZnO on Al and Cu) displayed superior boiling heat transfer characteristics compared against a bare Al and Si substrate. A 10X improvement in heat transfer coefficient was observed for nanostructured surfaces over a “bare” Al substrate. Further, an approximate 4X improvement in critical heat flux was also measured for these nanostructured surfaces. This work implies that these nanostructured surfaces create very high nucleation site densities and bubble frequency at the surface that leads to the high critical boiling heat fluxes, which in some cases approach theoretical maximums. This work also demonstrated a critical heat flux dependence on surface contact angle that suggests there is necessary balance between balance between the surface capillary fluid dynamics that brings fluid into the active nucleation sites and the surface bubble dynamics governed by bubble diameter and nucleation site density that ultimately lead to heat dissipation. This work hypothesizes a critical tradeoff is occurring between bubble frequency, nucleation site density and bubble diameter on these nanostructured

surfaces. Based on these encouraging results, testing these nano-structured surfaces on advanced microchannel architectures under forced liquid supply conditions is on-going.

ACKNOWLEDGMENTS

Authors wish to acknowledge and sincerely thank Mr. Don Higgins and Dr. Dan Palo for their invaluable assistance on this project. This research was sponsored by the Army Research Laboratory and was accomplished under Cooperative Agreement number W911NF-07-2-0083. The views and conclusions contained in this document are those of the authors and should not be interpreted as representing the official policies, either expressed or implied, of the Army Research Laboratory or the U.S. Government. The U.S. Government is authorized to reproduce and distribute reprints for Government purposes notwithstanding any copyright notation heron.

REFERENCES

1. I. Mudawar, Assessment of High-Heat-Flux Thermal Management Schemes, IEEE Transactions on Components and Packaging Technologies 24 (2) (2001) 122-140.
2. X. F. Peng, and G. P. Peterson, Convective Heat Transfer and Flow Friction for Water Flow in Microchannel Structures, International Journal of Heat & Mass Transfer 19(12) (1996) 2599-2608.
3. W. Qu, and I. Mudawar, Transport Phenomena in Two-Phase Micro-Channel Heat Sinks, Proceedings of the ASME International Mechanical Engineering Congress & Exposition, New Orleans, LA, (2002), Paper #IMECE2002-33711.
4. G. P. Celata, M. Cumo, M., and A. Mariani, Geometrical Effects on Sub-Cooled Flow Boiling Critical Heat Flux, Rev Gen Therm 36 (1997) 807-814.
5. A. Cavalini, L. Doretti, M. Marko, and L. Rossetto, Update on Condensation Heat Transfer & Pressure Drop Inside Minichannels, Heat Transfer Engineering 27 (4) (2006) 74-87.
6. Z. Y. Bao, D. F. Fletcher, and B. S. Haynes, Flow Boiling Heat Transfer of Freon R-11 and HCFC 123 in Narrow Passages, International Journal of Heat & Mass Transfer 43 (2000) 3347-3358.
7. A. Jacobi, and J. R. Thome, Heat Transfer Model for Evaporation of Elongated Bubble Flows in Microchannels, Journal of Heat Transfer 124 (2002) 1131-1136.
8. J. R. Thome, V. Dupont, V., and A. Jacobi, Heat Transfer Model for Evaporation in Microchannels, Part I: Presentation of the Model, International Journal of Heat & MassTransfer 47 (2004) 3375-3385.
9. R. Chen, M. Lu, V. Srinivasan, Z. Wang, H. H. Cho, and A. Majumdar, Nanowires for Enhanced Boiling Heat Transfer Nanoletters 9 (2) (2009) 548-553.
10. H. S. Ahn, N. Sinha, M. Zhang, D. Banerjee, S. Fang, S., and R. H. Baughman, Pool Boiling Experiments on Multiwalled Carbon Nanotube Forests Journal of Heat Transfer 128 (2006) 1335-1342.
11. C. Li, Z. Wang, P. I. Wang, Y. Peles, N. Koratkar, G. P. Peterson, Nanostructured Copper Interfaces for Enhanced Boiling, Small (2008) 1-5.

12. S. Ujereh, T. Fisher, and I. Mudawar, Effects of Carbon Nanotube Arrays on Nucleate Pool Boiling, International Journal of Heat and Mass Transfer 50 (2007) 4023-4038.
13. I. L. Pioro, W. Rohsenow, and S. S. Doerffer, "Nucleate Pool-Boiling Heat Transfer. I: Review of Parameteric Effects of Boiling Surface, International Journal of Heat and Mass Transfer 47 (2004) 5033-5044.
14. W. R. Gambill, and J. H. Lienhard, An Upper Bound for the Critical Boiling Heat Flux, Journal of Heat Transfer 111 (1989) 815-881.
15. Y.-J. Chang, P.-H. Mugdur, S.-Y. Han, A.A. Morrone, S.-O. Ryu, T.J. Lee, C.-H. Chang, Nanocrystalline CdS MISFETs Fabricated by a Novel Continuous Flow Microreactor, Electrochemical and Solid-State Letters 9(5) (2006) G174-G177.
16. Y. Chang, Y. Su, D. Lee, S. Ryu, and C.H. Chang, Investigate the Reacting Flux of Chemical Bath Deposition by a Continuous Flow Microreactor, Electrochemical Solid-State Letters 12 (7), (2009) H244-H247.
17. C. T. Tseng, and B.K. Paul, Comparison of Batch Mixing and Micromixing Approaches in the Synthesis and Deposition of Ceria Nanoparticles, Transactions of NAMRI 35 (2007).
18. S.-Y. Han, Y-J. Chang, D.-H Lee, S. –O Ryu, T. J. Lee, and C-H. Chang, Chemical Nanoparticle Deposition of Transparent ZnO Thin Films, Electrochemical and Solid-State Letters 10(1) (2007) K1-K5.
19. J. Y. Jung, N-K Park, T. J. Lee, S. -O Ryu, C-H. Chang, The growth of the flower-like ZnO structure using a continuous flow microreactor, Current Applied Physics 8 (2008) 720-724.
20. C. Chang, B.K. Paul, V.T. Remcho, S. Atre, J.E. Hutchison, Synthesis and post-processing of nanomaterials using microreaction technology, J Nanoparticle Research 10(6) (2008).
21. S. Liu, C-H Chang, High rate convergent synthesis and deposition of polyamide dendrimers using a continuous flow microreactor, Chemical Engineering Technology 30(3) (2007) 334–340.
22. P. H. Mugdur, Y.J. Chang, S.-Y. Han, Y.-W. Su, A.A. Morrone, S.O. Ryu, T.-J. Lee and C.-H. Chang, A comparison of chemical bath deposition of CdS from a batch reactor and a continuous-flow microreactor, Journal of Electrochemical Society 154(9) (2007) D482–D488.
23. S.-Y. Han, Y.-J. Chang, D.-H. Lee, S.O. Ryu, T.-J. Lee, C.-H. Chang, Chemical nanoparticle deposition of transparent ZnO thin films. Electrochem Solid-State Lett 10(1) (2007) K1–K5.
24. C. H. Wang, and V. K. Dhir, Effect of surface wettability on active nucleation site density during pool boiling of water on a vertical surface, Journal of Heat Transfer 115 (1993) 659-669.
25. S. P. Liaw and V. K. Dhir, Effect of surface wettability on transition boiling heat transfer from a vertical surface, Proc. Int. Heat Transfer Conf., San Francisco, 4 (1986) 2031-2036.
26. V. K. Dhir, Boiling Heat Transfer, Annual Review of Fluid Mechanics 36 (1998) 365-401.
27. T. G. Theofanous, J. P. Tu, A. T. Dinh, A. T., and T. N. Dinh, The boiling crisis phenomenon. Part I: Nucleation and nucleate boiling heat transfer, Experimental Thermal and Fluid Science, 26 (2002) 775-792.
28. R. E. Cavicchi and C. T. Avedisian Bubble nucleation and growth anomaly for a hydrophilic microheater attributed to metastable nanobubbles, Physical Review Letters 98 (2007) 124501.
29. E. Lauga, and M. P. Brenner, Dynamic mechanisms for apparent slip on hydrophobic surfaces, Physical Review E. 70 (2004) 026311.
30. P. G. De Gennes, On Fluid/Wall Slippage, Langmuir 18 (2002) 3413-3414.
31. V. P. Carey, Liquid-Vapor Phase-Change Phenomena, Taylor-Francis, Bristol, PA, (1992).
32. H. J. Chung, and H. C. No, A nucleate boiling limitation model for the prediction of pool boiling CHF, International Journal of Heat and Mass Transfer 50 (2007) 2944-2951.

33. H. Auracher, and W. Marquardt, Heat transfer characteristics and mechanisms along entire boiling curves under steady-state and transient conditions, International Journal of Heat and Fluid Flow 25 (2004) 223-242.

List of Figures

List of Tables

Table 1: Measured CHF values for repeat experiments

Surface – Contact Angle	**CHF (W/cm^2) – Test 1**	**CHF (W/cm^2) – Test 2**
Cu-ZnO (30°)	63.25	64.9
Cu-ZnO (10°)	43.4	35.07
Cu-ZnO (70°)	44.73	36.9
Al-ZnO (45°)	31.87	34.63

Table 2: Description of nano-structured surfaces

Legend/Symbol	Description	Average Surface Roughness (nm)
Al-ZnO-CA-0-CR	Zinc oxide nanoparticles on Al substrate with contact angle = 0°. Morphology of the nano-texture is “carpet-like”.	5863.2
Cu-ZnO-CA-10-FL	Zinc oxide nanoparticles on Cu substrate with contact angle = 10°. Morphology of the nano-texture is “flower-like”.	Not known
Al-ZnO-CA-18-UN	Zinc oxide nanoparticles on Al substrate with contact angle = 18°. Morphology of the nano-texture is “unique”.	258.03
Al-ZnO-CA-18-FL	Zinc oxide nanoparticles on Al substrate with contact angle = 20°. Morphology of the nano-texture is “flower-like”.	162.29
Cu-ZnO-CA-30-FL	Zinc oxide nanoparticles on Cu substrate with contact angle = 30°. Morphology of the nano-texture is “flower-like”.	183.64
Al-ZnO-CA-45-FL	Zinc oxide nanoparticles on Al substrate with contact angle = 45°. Morphology of the nano-texture is “flower-like”.	79.6
Bare Al	Bare Al plate with contact angle = 104°.	Not known

List of Figures

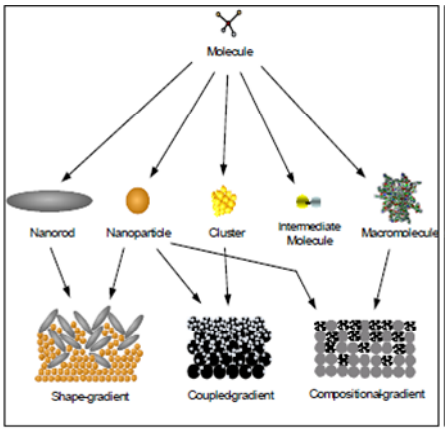

Figure 1: Various films enabled by Microreactor Assisted Nanomaterial Deposition (MAND^{TM}) based on nanoscale building.

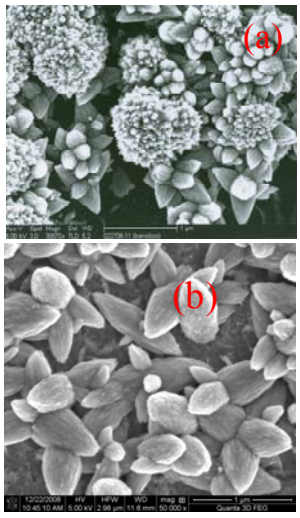

Figure 2: (a) ZnO on Al and (b) ZnO on Cu structures. Note the flower like morphologies produced by MAND process.

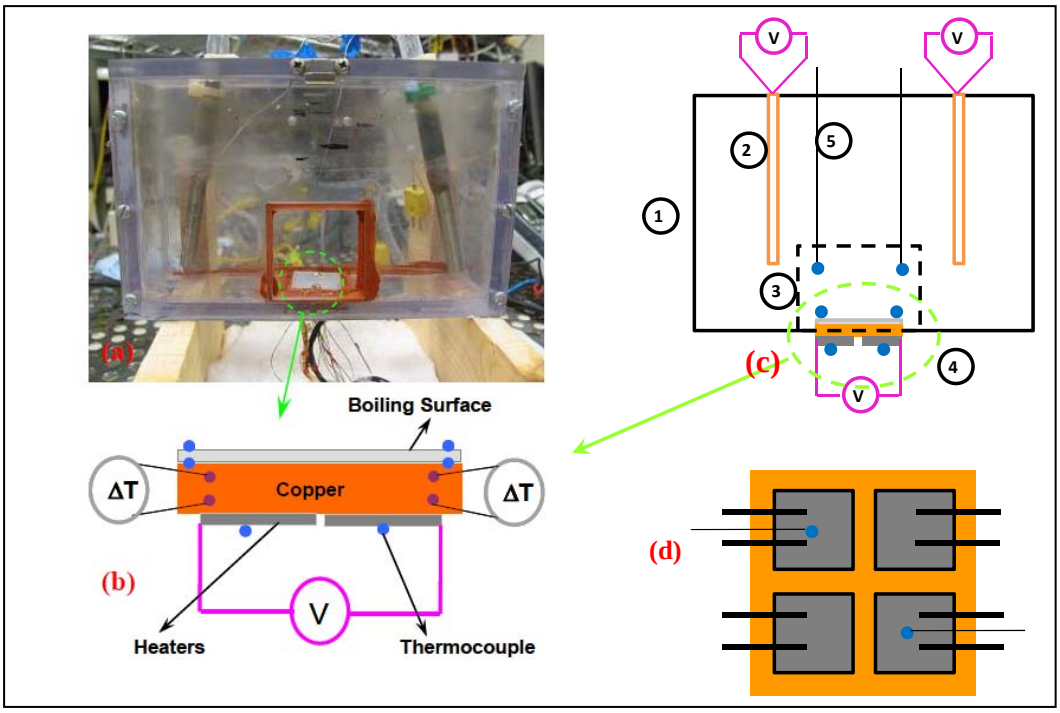

Figure 3: (a) Boiling test facility for pool-boiling performance characterization, (b) schematic illustration of the instrumented test heater set-up (filled blue circles are implemented thermocouples), (c) schematic of the boiling set-up (1: boiling chamber, 2: immersion heater, 3: visual window, 4: heating block, 5: thermocouple) , and (d) schematic of the heater assembly.

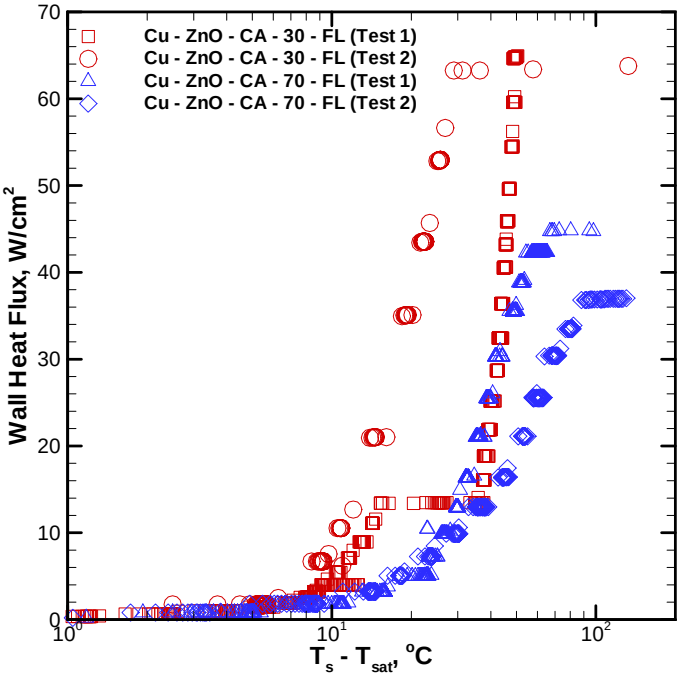

Figure 4: Pool boiling heat transfer comparison of repeat experiments for selected nano-textured surfaces.

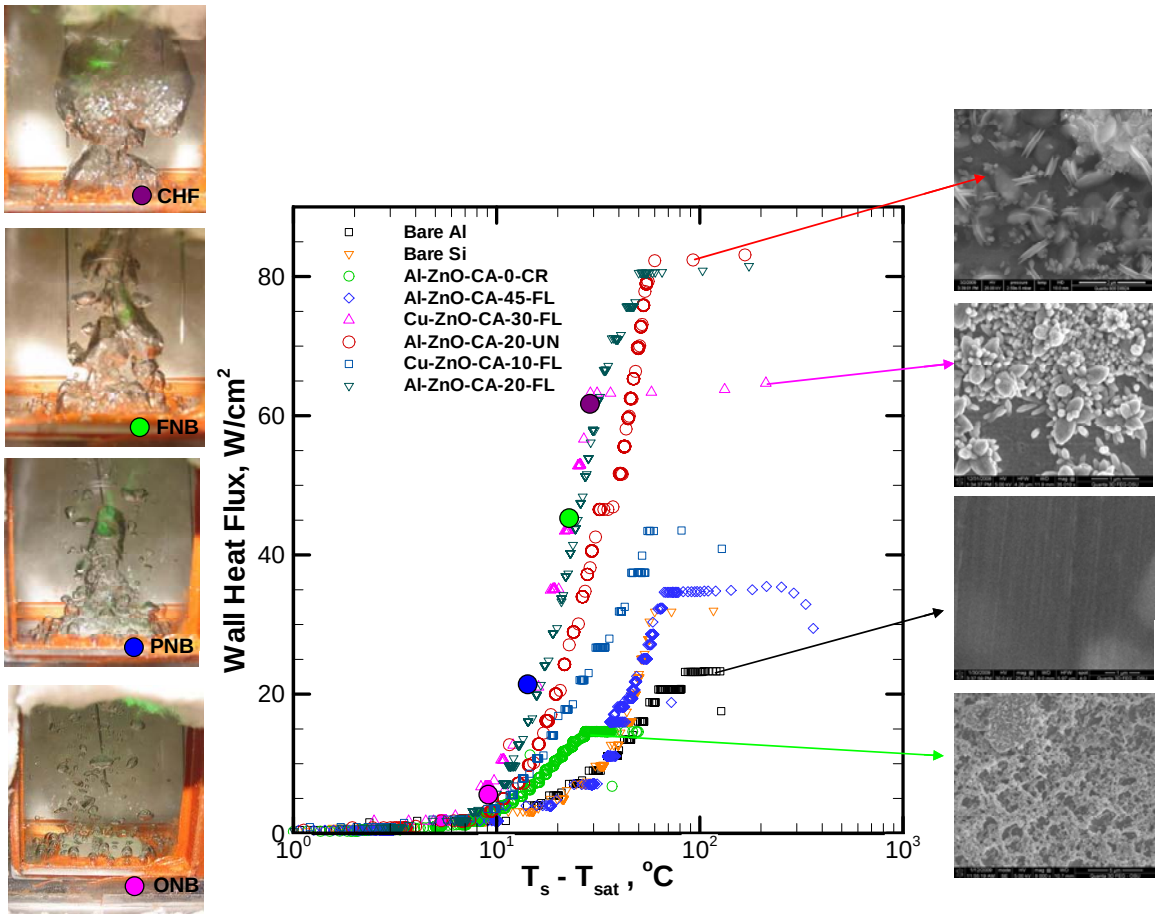

Figure 5: Pool boiling curves for nano-textured surfaces compared against bare Al and Si surfaces. Visual images of various pool boiling stages are highlighted on the left and their corresponding locations are highlighted as filled circles on Cu-30 Contact Angle boiling curve (ONB – Onset of Nucleate Boiling ⇒ PNB – Partial Nucleate Boiling ⇒ FNB – Fully-Developed Nucleate Boiling ⇒ CHF – Critical Heat Flux).

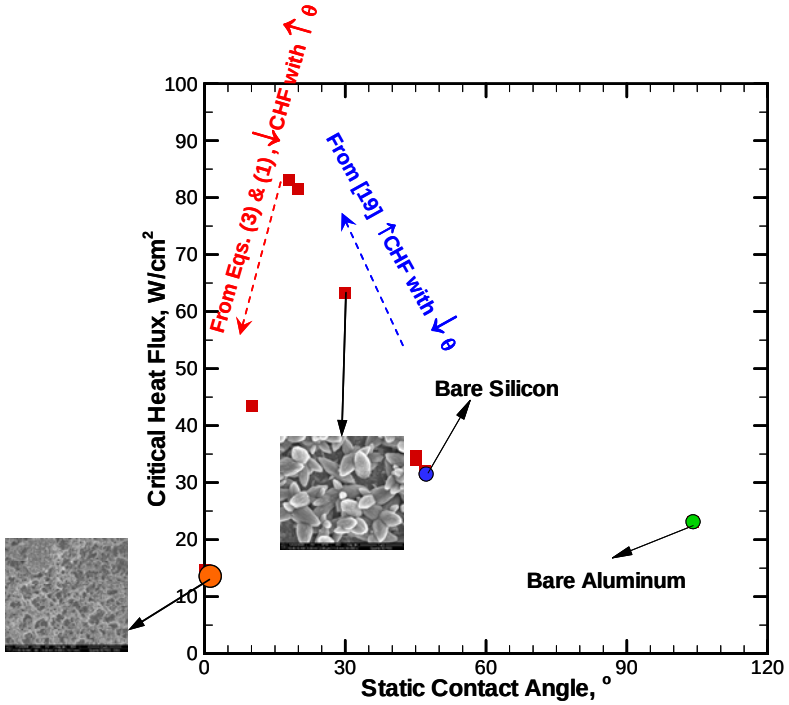

Figure 6: Measured critical heat flux as a function of static contact angle for nanostructured (red filled squares) and plain surfaces.

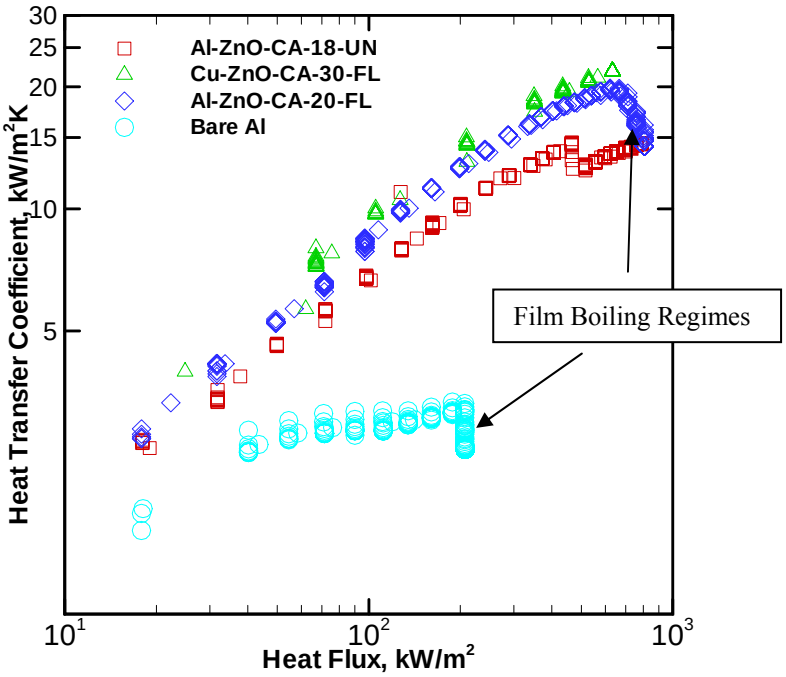

Figure 7: Measured heat transfer coefficient as a function of nucleate boiling heat flux (log-log plot).